Journal of Colloid and Interface Science 393 (2013) 397–401

Contents lists available at SciVerse ScienceDirect

Journal of Colloid and Interface Science

www.elsevier.com/locate/jcis

# Aerosol assisted fabrication of carbon nanotube/zinc oxide arrays for a field emission device

Jeong Hoon Byeon [a], Jang-Woo Kim [b,*]

[a] Department of Chemistry, Purdue University, IN 47907, United States
[b] Department of Digital Display Engineering, Hoseo University, Asan 336-795, Republic of Korea

ARTICLE INFO

*Article history:*
Received 18 July 2012
Accepted 29 October 2012
Available online 14 December 2012

*Keywords:*
Aerosol deposition
Zinc oxide nanoparticles
Carbon nanotubes
Arrays
Emission device

ABSTRACT

Aerosol deposition of zinc oxide (ZnO) nanoparticles was used to catalyze a silicon substrate site-selectively for a carbon nanotube (CNT) growth. An ambient spark discharge was used to produce aerosol ZnO nanoparticles, and the particle deposition on the substrate through a shadow mask was enhanced by thermophoresis. The ZnO-deposited substrate was then loaded into a chemical vapor deposition chamber, resulting in the formation of CNT/ZnO arrays. The turn-on field of an emission device constructed with the CNT/ZnO arrays was 1.7 V $\mu m^{-1}$ at a current of 2 μA, which was lower than that of the common CNT arrays.



## 1. Introduction

Carbon nanotubes (CNTs) have attracted much attention as promising field emitters because of their high aspect ratio, large field enhancement factor, and high electrical conductivity [1]. On the other hand, zinc oxide (ZnO) nanomaterials are shown to possess superior optoelectronic properties useful in nanoscale transistors, sensors, electron emitters, and many other systems [2]. CNT/metal oxide hybrids have drawn attention because metal oxides can modify the electronic structure of CNTs by virtue of charge transfer interactions as well as orbital hybridization at the junction [3]. The formation of heterojunctions of ZnO with CNTs should extend the scope of ZnO nanomaterials for potential applications [4]. In particular, the growth of aligned CNT/ZnO arrays remains a big challenge [5].

To grow CNT arrays using chemical vapor deposition (CVD) of hydrocarbons or other compounds, inert substrates must be catalyzed prior to CVD to provide a surface that can interact with carbon sources, enabling site-selective growth of CNTs [6]. Most of the pretreatment methods are based on lithographic techniques, and the use of laser, UV, plasma, and electron/ion beams have been reported [1,7–11]. However, these techniques require a quite expensive, high vacuum system, and precursor preparation [12]. It would be advantageous to activate the substrate surface through simpler, more effective, and more green means. From this viewpoint, the present investigation demonstrates a CNT array on a silicon substrate by replacing the traditional pretreatment with ZnO nanoparticles deposited from an aerosol, which does not contain expensive wet chemical and vacuum lithographic steps.

In this work, a CNT array was fabricated by producing aerosol ZnO nanoparticles using a spark discharge. Compared with other techniques, the use of a spark discharge is an attractive method because of the simplicity of the experimental setup, low impurity, and lack of need for complicated experiments. The ZnO nanoparticles were site-selectively deposited onto a silicon substrate through a shadow mask by thermophoresis, which is a physical phenomenon in which aerosol particles move across a temperature gradient [13–15]. The ZnO-deposited substrate was loaded into a CVD chamber to grow CNTs on the surface of ZnO. We further constructed a field emission device to examine electron emission from the fabricated CNT/ZnO arrays.

## 2. Materials and methods

The overall steps involving spark ZnO generation were used to grow CNTs on the surface of ZnO nanoparticles and they are schematically described in Fig. 1a. The method involves the generation of aerosol ZnO particles *via* spark discharge [16,17] and their thermophoretic deposition on a silicon substrate (N-type (100), resistivity of $10^{-2}$–$10^{-3}$ Ω cm) through a stainless steel shadow mask (hole diameter 1 μm, depth 30 μm, Youngjin Astech, Korea).

The temperature of the particle-laden flow was maintained at 22 °C with a tube heater, and the temperature of the silicon substrate was maintained at 4 °C, thereby enhancing deposition of the particles onto the substrate *via* thermophoresis [18]. Computational

* Corresponding author. Fax: +82 41 540 5925.
*E-mail address:* jwkim@hoseo.edu (J.-W. Kim).

0021-9797/$ - see front matter © 2012 Elsevier Inc. All rights reserved.
http://dx.doi.org/10.1016/j.jcis.2012.10.068

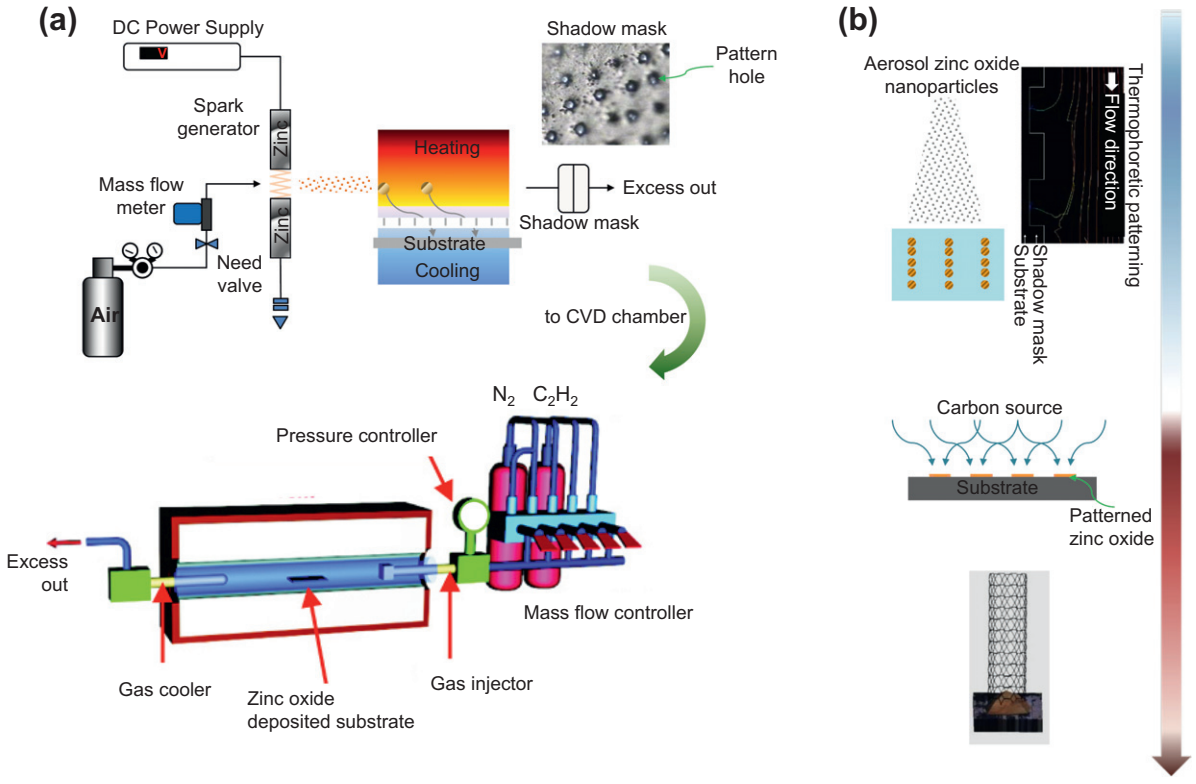


**Fig. 1.** (a) Schematic diagram of CNT/ZnO arrays fabrication apparatus used for this work. (b) CNT growth on site-selectively deposited ZnO nanoparticles.

fluid dynamics (CFD, Fluent 6.3, Ansys, US) calculations were performed with particle trajectories and a temperature distribution in a thermophoretic deposition chamber (Fig. 1b). Thermophoretic velocities were calculated according to the expression for the particles, with Knudsen's number >3:

$$v_{\mathrm{th}} = -\frac{3}{8}\frac{\mu_g \nabla T}{0.499\rho_g T_g(1+\pi\alpha/8)} = -K_{\mathrm{th}}\frac{\mu_g \nabla T}{\rho_g T_p} \quad (1)$$

where $\nabla T$ represents the temperature gradient in the vicinity of the particle, $\alpha$ is the accommodation coefficient, and $K_{\mathrm{th}}$ (=0.54) is the numerical coefficient estimated at $\alpha = 1$ [19], which increases with decreasing particle size. As shown in Fig. 1b, the particles were expected to be deposited on the silicon substrate by thermophoresis due to the temperature gradient. The substrate was then separated from the shadow mask and loaded into a CVD chamber to grow CNTs on the ZnO particles. As the temperature was increased to 650 °C, nitrogen gas was injected at 100 mL min$^{-1}$ through the chamber to clean the inside of the chamber. The pressure inside the chamber was 2.7–4.5 Torr. When the temperature stabilized, the carrier gas was replaced by acetylene gas at 30 mL min$^{-1}$ for 10 min. After the synthesis of the CNTs was finished, the chamber was cooled to room temperature in a nitrogen ambient environment.

## 3. Results and discussion

The size distributions of the ZnO nanoparticles were measured using a scanning mobility particle sizer (SMPS, 3936, TSI, US), and the results are provided in Fig. 2a. The total number concentration, geometric mean diameter, and geometric standard deviation of the spark generated particles were $9.74 \times 10^6$ particles cm$^{-3}$, 43.4 nm, and 1.57, respectively. X-ray diffraction (XRD, RINT-2100, Rigaku, Japan) results for the spark generated particles demonstrated the formation of crystalline ZnO of hexagonal lattice structures ($a$ = 0.325 nm and $c$ = 0.521 nm), depicted in Fig. 2b. The obtained spectra had the first ZnO main peaks at $2\theta$ = 31.6, 34.3, 36.2, 43.2, 47.4, 56.6, 62.7, 66.5, 67.9, 68.9, 72.5, and 76.9°. The measured $c/a$ ratio (1.62) was in good agreement with that for the ideally close-packed hexagonal structures ($c/a$ = 1.63). From the width of the (002) peak by using Scherrer's equation, the average size of the crystallite forming grain was determined to be 16.4 nm. The size obtained by the SMPS was bigger than the size obtained from XRD. In fact, the particle size in XRD represented the average size of the crystallites and not that of the generated particles. This shows that the generated particles were polycrystalline in nature. The morphology and structure of the particles were characterized by a transmission electron microscope (TEM, 3010, JEOL, Japan) and fast Fourier transformation (FFT) pattern (Fig. 2c). The TEM images revealed that the morphology of the ZnO particles consisted of agglomerates of several primary particles, and thus, a direct size determination was difficult from the images. It was clear that the primary particles were touching each other, and this touching was a probable source for twinning planes in the ZnO particles (inset, right). The presence of a high temperature region and air flow in the generation led to the formation of a temperature gradient and a fast condensation process [20]. This gradient may mostly generate the agglomerates of primary particles because there was no enough time to form well-defined (e.g. rod) structures before stabilization. The corresponding FFT pattern (inset, left) shows both splitting and streaking of the diffraction spots, which confirmed the presence of twinning characteristics in the particles. The optical bandgap, $E_g$, of the particles was determined using the following equation:

$$\alpha h\nu = (h\nu - E_g)^{1/2} \quad (2)$$

where $\alpha$ is the optical absorbance coefficient and $h\nu$ is the photon energy. By plotting $(\alpha h\nu)^2$ as function of $h\nu$ as shown in Fig. 2d, and extrapolating the linear portion of the curve to an absorption

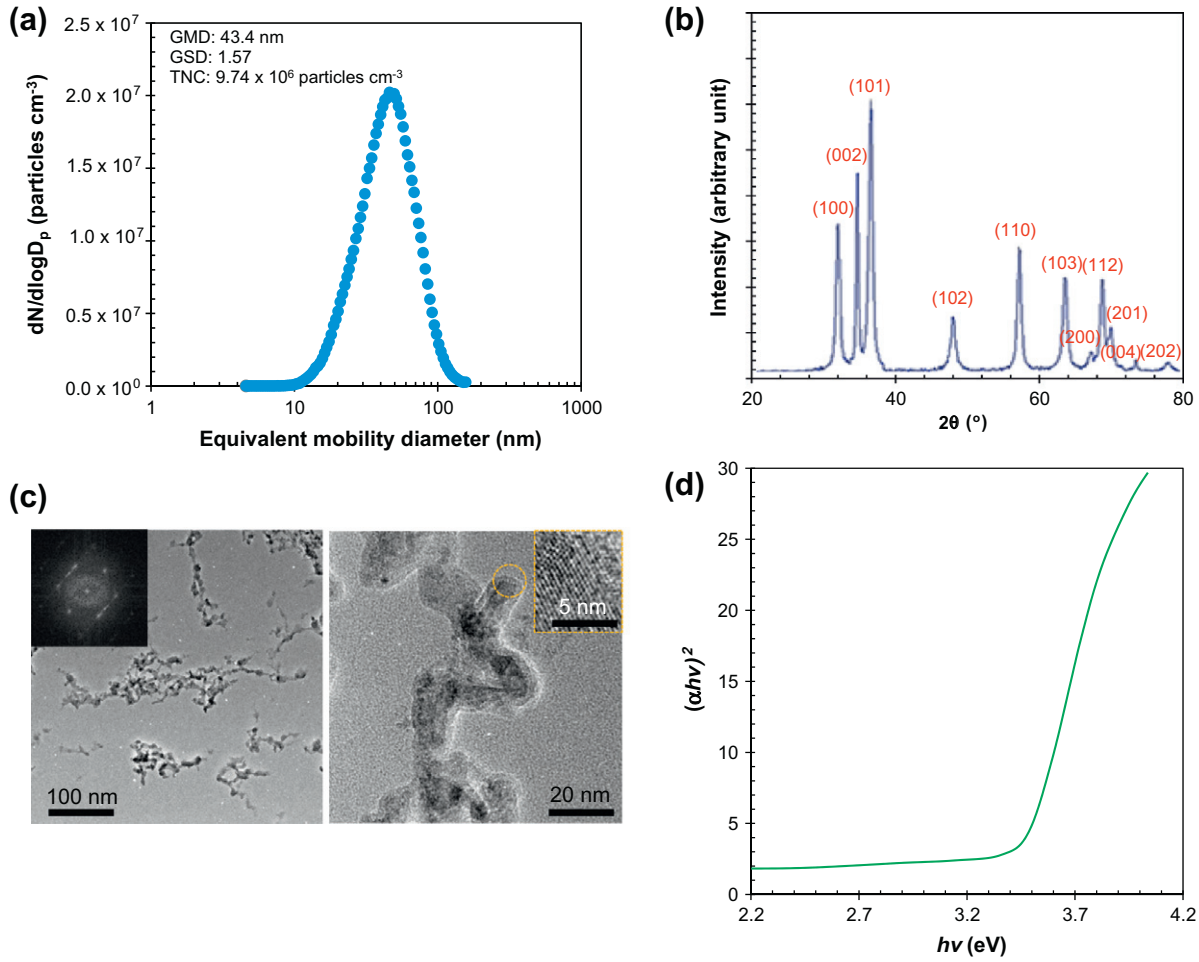


**Fig. 2.** Results for spark generated ZnO nanoparticles. (a) Size distribution of the aerosol ZnO particles. (b) XRD pattern of the ZnO particles. (c) TEM images and FFT pattern of the ZnO particles. (d) $(\alpha h\nu)^2$ vs. $h\nu$ diagram for the ZnO particles.

equal to zero the values of the direct optical bandgap energy for the generated ZnO particles were estimated. The $\alpha$ term was evaluated from the absorbance, $D$, and thickness, $l$, according to the relation $\alpha = D/0.43l$, and thereby, the bandgap was estimated to be approximately 3.38 eV.

Fig. 3a shows scanning electron microscope (SEM, LEO-1530, Carl Zeiss, Germany) images of the CNT growth on differently deposited ZnO particles after CVD. The CNTs grew in random directions with diameters of less than ~30 nm. The random growth of the CNTs may have originated from the twinning facets of the ZnO particles as described in Fig. 2c. The increase in CNT growth upon increasing the ZnO deposition time from 5 to 30 min can be explained by considering the ZnO density on the substrate. A previous study reported that increased CNT growth could be related to larger or more densely placed catalyst particles [21]. The ZnO particles effectively acted as catalysts to initiate the CNT growth. The process was hence clearly observed to occur by the initial growth at several sites on the ZnO, followed by the diffusion of carbon sources toward the growing graphitic islands and the construction of CNTs on the ZnO particles. As also shown in Fig. 3a, the CNT growth occurred only on the ZnO particles, i.e. at the ZnO deposited region of the substrate. Fig. 3b shows SEM images of the CNT/ZnO stripe pattern on the substrate from a different shadow mask. The CNT was densely grown on the stripe pattern, and this implies that the present method is sufficiently versatile to fabricate various configurations of CNT/ZnO arrays. Typical TEM (Fig. 3c) and Raman spectroscopy (Fig. 3d) were also used to investigate the structure of the CNTs. For these purposes, the CNTs were separated from the substrate by sonication in ethanol, and the CNT-containing solution was dropped onto a TEM grid. Fig. 3c shows the hollow structure (~10 nm diameter) inside the multi-walled graphitic layers (~20 nm thickness). The ZnO particles with diameters greater than 10 nm introduced a growth of multi-walled CNTs [22]. The Raman spectrum of the CNTs shows two main peaks centered at 1338 $cm^{-1}$ ($D$ band) and 1575 $cm^{-1}$ ($G$ band). The $G$ peak was due to bond stretching of all pairs of $sp^2$ carbon atoms in both the rings and chains, while the $D$ peak was due to the breathing modes of the rings. The intensity ratio ($I_G/I_D$) between the $G$ and $D$ bands was ~0.65, indicating the presence of a larger amount of $sp^3$ carbon than $sp^2$ carbon. This implies that the CNT growth on the ZnO particles shows a multi-walled structure with defective graphitic sheets on the walls.

After confirming that the CNTs were grown on the ZnO particles, we constructed a field emission device to examine electron emission from the CNT/ZnO arrays. The constructed device structure is illustrated in Fig. 4a. A 300 μm-thick insulating spacer with a 2.25 $cm^2$ window was placed on the CNT/ZnO arrays (as the cathode), and an indium tin oxide (ITO) glass plate (as the anode) coated with phosphor (ZnS: Cu, Al) was placed on the spacer. A voltage was applied to the device in a vacuum chamber (~$10^{-5}$ Pa), and the light emission from the device was monitored. Fig. 4a also shows a photographic image of the light emission from the device at an applied voltage of 1 kV. Some spatially non-uniform emissions were also seen, which was probably due to an

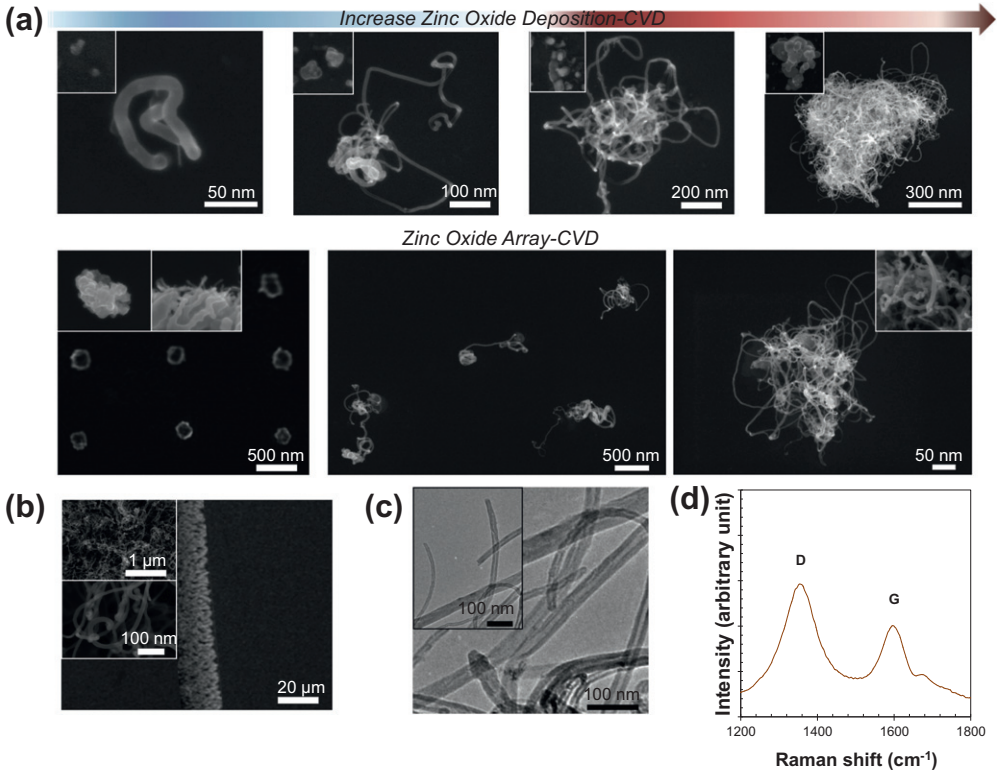


**Fig. 3.** Results for the fabrication of CNT/ZnO arrays. (a) SEM images for CNT growth on differently deposited ZnO particles (insets) and ZnO arrays (bottom line). (b) SEM images for CNT growth on a ZnO stripe pattern. (c) TEM images of the grown CNTs. (d) Raman spectra of the grown CNTs.

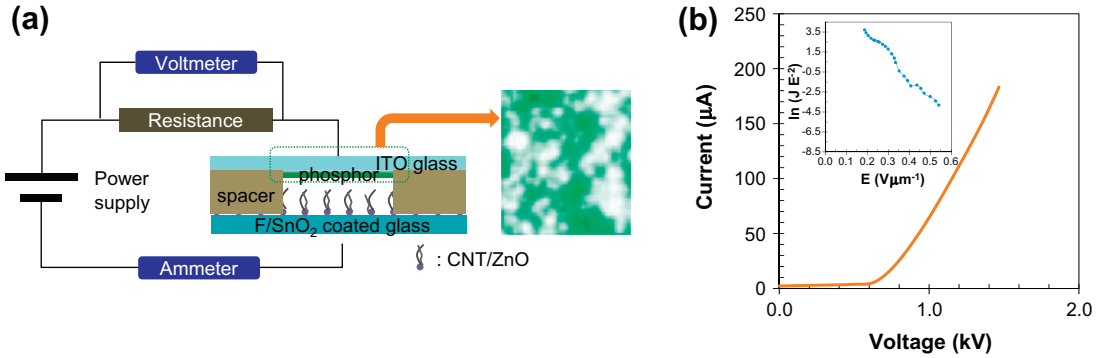


**Fig. 4.** (a) Schematic diagram of the field emission device. (b) Field emission current–voltage curve of the device. Inset is the corresponding F–N plot.

inhomogeneity of the CNT distribution. The turn-on voltage of the device was 515 V. Since the space between the cathode and the anode was 300 μm, the turn-on field of the device was ~1.7 V μm$^{-1}$ at a current of 2 μA (Fig. 4b), which was lower than that of the common CNT arrays (~2.5 V μm$^{-1}$) [7]. Electrons transported through the bond between the CNTs and ZnO into the conduction band of the ZnO cause the increasing carriers to enhance the field emission current density. When the electrical field reached the turn-on field, most of the emission sites would contribute to the current. Inset of Fig. 4b shows a Fowler–Nordheim (F–N) plots for the CNT/ZnO arrays, and it fit well to the linear relationship given by $\ln(JE^{-2}) = \ln(A\beta^2\varphi^{-1}) - B\varphi^{3/2}\beta^{-1}E^{-1}$, which indicates that the measured current is mostly due to vacuum tunneling from CNT/ZnO arrays, where $A = 1.54 \times 10^{-6}$ A eV V$^{-2}$, $B = 6.83 \times 103$ eV$^{-3/2}$ V μm$^{-1}$, $\beta$ is the field enhancement factor, and $\varphi$ is the work function of emitters [23]. Since ZnO has a higher work function (5.3 eV) than that of CNT (5.0 eV), it is possible to make an ohmic contact to CNT [24,25]. Based on the work function of CNT and ZnO, the $\beta$ is calculated to be 2884 for CNT/ZnO arrays. Moreover, the results were comparable to previous reports for estimations of the corresponding F–N plot at CNT/ZnO structures [23,24,26].

## 4. Conclusions

The fabrication of CNT/ZnO arrays on silicon substrate was performed using spark generated ZnO nanoparticles. The aerosol ZnO particles were deposited onto the silicon substrate under thermophoretic attraction between the particles and the substrate. The ZnO-deposited substrate was then loaded into a CVD chamber, resulting in the growth of CNT on the previously deposited ZnO of the substrate. The turn-on field of the emission device constructed with the CNT/ZnO arrays was 1.7 V μm$^{-1}$ at a current of 2 μA,

which was lower than that of the common CNT arrays ($\sim$2.5 V $\mu m^{-1}$). The process is versatile, cost-effective, and generalizable, and can be applied in order to produce field emitters and electro-optic sensors.

## References


[1] G.-H. Jeong, N. Olofsson, L.K.L. Falk, E.E.B. Campbell, Carbon 47 (2009) 696.
[2] N. Tarasenko, A. Nevar, M. Nedelko, Phys. Status Solidi A – Appl. Mater. 207 (2010) 2319.
[3] K. Ghosh, M. Kumar, H. Wang, T. Maruyama, Y. Ando, Langmuir 26 (2010) 5527.
[4] J. Chang, C.K. Najeeb, J.-H. Lee, M. Lee, J.-H. Kim, J. Phys. D – Appl. Phys. 44 (2011) 095101.
[5] J. Liu, X. Li, L. Dai, Adv. Mater. 18 (2006) 1740.
[6] S.-F. Lee, Y.-P. Chang, L.-Y. Lee, J. Vac. Sci. Technol. B 26 (2008) 1765.
[7] S. Zuo, X. Li, Y. He, Z. Xiao, C. Zhu, J. Nanomater. 2011 (2011) 382068.
[8] X. Yan, B.-K. Tay, P. Miele, Carbon 46 (2008) 753.
[9] J. Im, I.-H. Lee, B.Y. Lee, B. Kim, J. Park, W. Yu, U.J. Kim, Y.H. Lee, M.-J. Seong, E.H. Lee, Y.-S. Min, S. Hong, Appl. Phys. Lett. 94 (2009) 053109.
[10] S. Huang, A.W.H. Mau, T.W. Turney, P.A. White, L. Dai, J. Phys. Chem. B 104 (2000) 2193.
[11] H. Ago, J. Qi, K. Tsukagoshi, K. Murata, S. Ohshima, Y. Aoyagi, M. Yumura, J. Electroanal. Chem. 559 (2003) 25.
[12] C.-C. Chiu, M. Yoshimura, K. Ueda, Diam. Relat. Mater. 18 (2009) 355.
[13] J.H. Byeon, J.H. Park, K.Y. Yoon, J. Hwang, Langmuir 24 (2008) 5949.
[14] J.H. Byeon, K.Y. Yoon, Y.K. Jung, J. Hwang, Electrochem. Commun. 10 (2008) 1272.
[15] J.H. Byeon, J.T. Roberts, ACS Appl. Mater. Interfaces 4 (2012) 2515.
[16] J.H. Byeon, J.H. Park, J. Hwang, J. Aerosol Sci. 39 (2008) 888.
[17] J.H. Byeon, J.-W. Kim, ACS Appl. Mater. Interfaces 2 (2010) 947.
[18] D. Gonzalez, A.G. Nasibulin, A.M. Baklanov, S.D. Shandakov, D.P. Brown, P. Queipo, E.I. Kauppinen, Aerosol Sci. Technol. 39 (2005) 1064.
[19] N.A. Fuchs, The Mechanics of Aerosols, Pergamon Press, Oxford, UK, 1964.
[20] J.H. Byeon, J.-W. Kim, Appl. Phys. Lett. 96 (2010) 153102.
[21] M.J. Bronikowski, Carbon 44 (2006) 2822.
[22] C.L. Cheung, A. Kurtz, H. Park, C.M. Lieber, J. Phys. Chem. B 106 (2002) 2429.
[23] Y.M. Ho, W.T. Zheng, Y.A. Li, J.W. Liu, J.L. Qi, J. Phys. Chem. C 112 (2008) 17702.
[24] C. Li, G. Fang, L. Yuan, N. Liu, L. Ai, Q. Xiang, D. Zhao, C. Pan, X. Zhao, Nanotechnology 18 (2007) 155702.
[25] N. Liu, G. Fang, W. Zeng, H. Long, X. Zhao, J. Phys. Chem. C 115 (2011) 14377.
[26] C.-S. Huang, C.-Y. Yeh, Y.-H. Chang, Y.-M. Hsieh, C.-Y. Ku, Q.-T. Lai, Diam. Relat. Mater. 18 (2009) 452.